Organization of Storm Track Anomalies by Recurring Low-Frequency Circulation Anomalies

GRANT BRANSTATOR

National Center for Atmospheric Research, Boulder, Colorado*

(Manuscript received 21 February 1994, in final form 31 May 1994)

ABSTRACT

From previous studies it is known that anomalous momentum fluxes by bandpass eddies are important in maintaining long-lasting tropospheric flow anomalies. Evidence is presented that suggests that these anomalous fluxes do not occur at random but happen because the structure of storm track activity is modified by the presence of prominent low-frequency, large-scale circulation anomalies. This behavior is noted in an extended integration of a perpetual January simulation with a general circulation model (GCM).

Because nonlinear feedbacks between low- and high-frequency variability make it difficult to establish causal relationships between these two ranges of variability, a model is constructed that approximates the storm track activity that would be expected to accompany a given low frequency without including the feedback of the high frequencies onto the low-frequency state. This model is based on the linearized primitive equations and uses a series of short integrations from random initial conditions to establish the statistics of the storm tracks. After first tuning this model to reproduce the storm tracks of the GCM climate, the model is verified by applying it to other climate states. Next it is used to determine the perturbations to the climatological storm track that result because of the presence of two prominent low-frequency anomalies that are observed to frequently occur in the GCM. The storm track anomalies that are caused by these low-frequency anomalies match the storm track anomalies that accompany the low-frequency anomalies in the GCM, thus establishing that in the GCM the low-frequency patterns cause the coincident storm track anomalies.

Further experiments with the linear storm track model help to pinpoint which processes are important in organizing the storm track structure. It turns out that the barotropic component of the low-frequency disturbances has a large impact on the high-frequency disturbances. Group velocity calculations indicate that the barotropic component affects the distribution of storms by steering, rather than stretching and straining, the perturbations. Calculations also demonstrate that because the distribution of storms in the climatological state is nonuniform, some large-scale patterns may be able to organize storm track activity in such a way that the associated momentum fluxes positively feed back onto the large-scale anomalies while other patterns cannot induce such a positive feedback.

The study concludes that since a two-way feedback has now been demonstrated between high- and low-frequency disturbances during episodes of prominent anomalies, the two timescales are inseparable and the description of recurring anomalies is incomplete without inclusion of the fast timescale fields. It is also suggested that the storm track model used in the study may serve as a useful means of parameterizing fluxes by bandpass perturbations in low-frequency models of the atmosphere.

1. Introduction

Based on general circulation model studies like that of Lau (1981) and the results of integrations with simplified dynamical models like those of Hendon and Hartmann (1985), it is well established that large-scale, long-lasting flow anomalies can be produced in the atmosphere even without the influence of slowly varying boundary conditions. Analyses of such experiments have made it clear that an important contributor to the maintenance of such flow anomalies is forcing from anomalous distributions of momentum fluxes by bandpass eddies that occur during episodes of the low-frequency circulation anomalies. This has been found to be true in both general circulation models [as in the work of Branstator (1992) and Ting and Lau (1993)] and simpler models [as described by Vautard and Legras (1988), Cai and Mak (1990), and Robinson (1991)]. Examples of this are the two patterns of Figs. 1a,b, which are essentially the same structures whose maintenance was examined by Branstator (1992). These patterns, hereafter referred to as patterns A and B, were produced in a 200-month perpetual January

* The National Center for Atmospheric Research is sponsored by the National Science Foundation.

Corresponding author address: Dr. Grant Branstator, NCAR, P.O. Box 3000, Boulder, CO 80307-3000.

simulation with an R15, nine-level National Center for Atmospheric Research general circulation model (GCM).[1] As explained in the figure caption, they are composites based on an empirical orthogonal function analysis of monthly mean 300-mb streamfunction fields. Figures 1c,d show composites of the anomalous variance of 1–7 day bandpass streamfunction at an upper-tropospheric level for those months when the two patterns are prominent. This band of variance is commonly, if erroneously, referred to as the atmosphere's storm track activity. In the regions where the flow anomalies are strong, the storm track activity is shifted from its normal position. Furthermore, as depicted in Figs. 1e, f, the streamfunction tendency produced by the anomalous vorticity fluxes associated with these changes in the storm tracks has a structure that is similar to the circulation anomalies and might be expected to help maintain them. Solutions of a linearized version of the GCM when forced by these anomalous fluxes indicate that they do maintain patterns A and B (Branstator 1992). This is similar to the situation that has been found for blocks in nature (Illari 1984) and in models (Shutts 1983; Mullen 1987) and for low-frequency teleconnection patterns in observations (Lau 1988; Metz 1989; Trenberth and Hurrell 1994).[2] In this paper we are concerned with identifying mechanisms that produce organized, long-lived anomalies in the storm tracks, like those in Figs. 1c and 1d, and which by so doing help to stimulate structures like patterns A and B.

The exact position, strength, and structure of individual storms is so sensitive to so many factors that the statistical properties of the disturbances that occur during any given period may have a substantial stochastic component. If this stochastic component is large enough, the occurrence of the storm track anomalies in Fig. 1 may be thought of as random events. Even if they occur randomly, particular storm track patterns could appear in the composites because they happen to force a resonant response, namely, patterns A or B. Such an interpretation of why certain storm track anomalies coincide with events of prominent flow anomalies is along the lines of the Egger and Schilling (1983) notion, as modified by Branstator (1990), that a system with linear quasigeostrophic dynamics when randomly forced will produce low-frequency variance whose structure is similar to that observed because those structures with low natural frequencies will tend to resonate with the low-frequency component of the random forcing.

Though the view that recurring persistent patterns are the result of chance anomalies in fluxes from bandpass disturbances qualitatively matches observed behavior, it has two shortcomings. First, from studies by Lau (1988) and Metz (1989), we know that the bandpass eddies are not random but rather are highly organized on monthly timescales. Second, this notion seems unable to quantitatively account for the structure and frequency of appearance of low-frequency anomalies. With the GCM climate for a background state and forced with steady vorticity sources that were random in space, Branstator (1990) found that his linear model tended to produce patterns that shared the same arching characteristics of the GCM's leading low-frequency anomalies (i.e., patterns A and B), but a pattern with the exact position and structure of A was not commonly stimulated (see Fig. 7 of Branstator 1990). However, if that same linear model is forced by each of the 200 distributions of monthly mean vorticity fluxes by bandpass transients that occurred in the GCM simulation used to define A and B, then the resulting 200 steady solutions do have patterns A and B as recurring patterns. This can be seen in Fig. 2, which shows two linear combinations of the leading two empirical orthogonal functions of streamfunction at level $\sigma = .336$ from these 200 solutions. The similarity in structure between these patterns, which together explain 56% of the variance in the 200 linear solutions, and patterns A and B is unmistakable. The increase in similarity between the linearly forced structures and the GCM structures, when the linear model is forced by the fluxes from actual distributions of transients rather than randomly, suggests that these fluxes are not occurring strictly by chance but are organized by some mechanism, and this organization is essential to the maintenance of prominent low-frequency anomalies.

In this paper we will consider the possibility that the primary means by which anomalous storm track organization is produced is the influence that large-scale, low-frequency anomalies have on the smaller, fast timescale eddies through their modification of the steering currents and the regions of intense baroclinity. Note that this interaction between slow and fast timescale disturbances is the opposite of that discussed in the above maintenance studies; here the slow timescales are influencing the behavior of the fast timescales rather than the fast timescales forcing the slow perturbations. This direction of influence has been discussed by synopticians for decades (see Namias 1953; Pettersen 1956) and has been considered for blocking by Dole (1986) and Shutts (1983), for long-lived anomalies in the simple model studies mentioned earlier, and for per-

[1] The GCM used in this study is version 0B of the NCAR Community Climate Model. It has been described by Williamson (1983).

[2] The relationship between the momentum fluxes by transients and the time mean eddies in Fig. 1 is also reminiscent of the climatological flow in nature. There, as Lau and Wallace (1983) have argued, upper-tropospheric fluxes by transients tend to balance the drag on the atmosphere caused by surface stresses and communicated to upper levels by Ekman-induced secondary circulations. Plots of surface pressure anomalies associated with patterns A and B (not shown) indicate that indeed the tendencies in Figs. 1e,f would counteract the anomalous drag on the atmosphere associated with these patterns.

sistent anomalies in nature by Robertson and Metz (1989, 1990).

Because low-frequency quantities are simultaneously influencing and being influenced by bandpass quantities, it is difficult to establish how one timescale is affecting the other. In the maintenance study of Branstator (1992), this difficulty was overcome by considering the influence of the bandpass eddies on slow timescale anomalies in a linear setting in which the feedback of the low-frequency anomalies onto the transients was not included. In the current study we use a similar strategy. The influence of the slowly evolving component of the circulation on the bandpass disturbances is studied in a linear model in which the feedback of the bandpass transients onto the low frequencies is not allowed and in which transient eddy structure and distribution is solely determined by the structure of an assumed background state. This approach, which is described in section 2, is related to the eigenvalue/eigenvector method that Reinhold and Pierrehumbert (1982) and Cai and Mak (1990) successfully used to determine the influence of large-scale anomalies on small-scale perturbations in their simple dynamical models, but unlike that method it does not rely on just a few modes to represent the fast timescales. As demonstrated in section 2, even though nonlinear mechanisms are missing, the model is quite successful at reproducing the geographical distribution of variance and fluxes associated with a variety of climatological storm tracks in a GCM and in nature.

Having validated the linear storm track model's ability to indicate the bandpass statistics that occur as the result of a given background state, we apply it to the question of the organization of storm track anomalies. In section 3 we use it to study patterns A and B and find that indeed the effect of these anomalies on the storm tracks is to produce anomalous variance and fluxes with the same structure as those observed to coincide with episodes of those two patterns. In section 4 we present further experiments with the linear model of the storm tracks that help elucidate which attributes of the system are important in determining the influence of low-frequency anomalies on the distribution and structure of bandpass eddies.

In addition to establishing that storm track anomalies associated with prominent low-frequency patterns are caused by those patterns, the results of our study have several implications. They are discussed in section 5, where we point out that since feedbacks between low-frequency and bandpass perturbations have been found in both directions, there is the possibility of positive feedbacks that would serve as a means of natural selection of low-frequency anomalies. We also suggest that the linear model of storm tracks used in this investigation may prove to be an effective parameterization of transient eddies and their associated fluxes.

2. Linear model of storm tracks

a. Model formulation and tuning

Frederiksen (1982) has demonstrated that when linearized about the observed three-dimensional time mean state, the fastest growing modes of a quasigeostrophic model tend to have variance that is concentrated in the same regions that bandpass transients tend to be concentrated in observational studies. Frederiksen (1989), when studying blocking situations, and Robertson and Metz (1989, 1990), when considering persistent anomalies, have found that the structures of the most unstable modes of such a model are modified when the model background state includes a low-frequency anomaly. The modification to the modes is similar to the changes in bandpass eddies that are observed during episodes of the persistent anomalies. For our study we need a model that indicates the storm track that would form for a given time mean flow without the inclusion of the eddy feedback. The results of Frederiksen and Robertson and Metz lead us to suspect that a linear model like the ones they used may satisfy this need. With such a model there is a clear cause and effect relationship between slow and fast timescale disturbances; any correspondence between slow and fast timescale anomalies must be the result of slow perturbations influencing the behavior of fast perturbations.

To determine the transients that the equations of a linear model imply would be expected to occur in the presence of a given time mean state, we could use the technique employed by others and examine the one or two most unstable modes of the model when it is linearized about that state. This method has been successful when qualitative information is sought or when a system with a limited number of degrees of freedom is being analyzed, but when applied to more complicated systems, researchers have encountered difficulties. The primary difficulty is that in more realistic systems examination of just one or two modes is not sufficient to characterize the system because, as the calculations of Frederiksen (1983) make clear, there are numerous unstable modes, many with similar growth rates. Another problem is that the system is not self-adjoint so that the likelihood that perturbations will project onto each mode must be taken into account when determining which modes will tend to be most instrumental in determining the evolution of the system. Furthermore, if one is interested in the behavior of disturbances with timescales of a few days, Farrell (1989) has pointed out that the fastest growing normal modes may not be the most important structures. To overcome these difficulties with the eigenvalue/eigenvector approach, we use an initial value technique instead. Starting from a spatially white random distribution of perturbations, a linear model is integrated for several days to determine how disturbances would tend to evolve under the influence of the basic state. Feeling

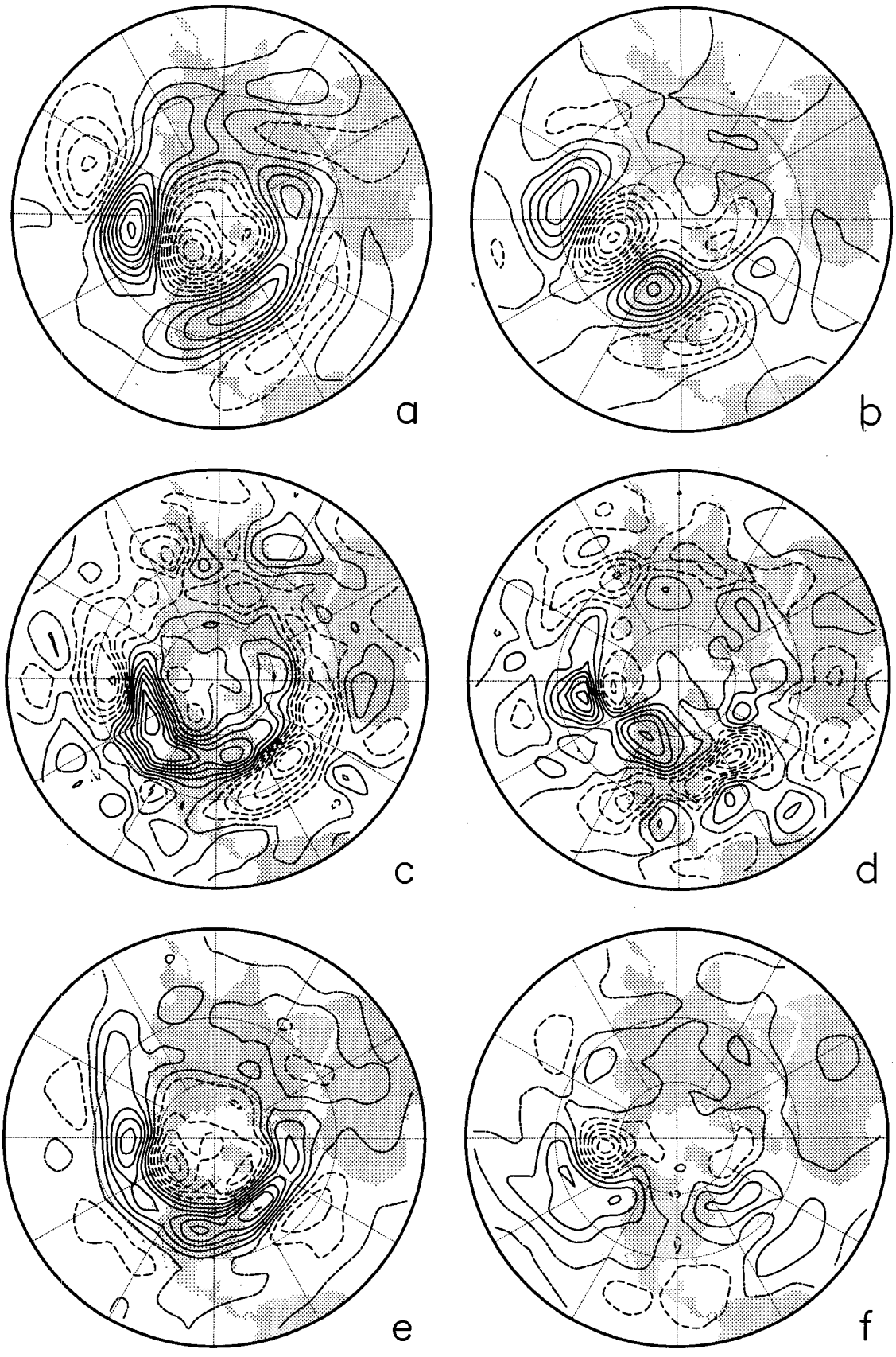
a
b
c
d
e
f

the effects of local regions of baroclinity and the steering effect of the background winds, there is a tendency for perturbations with certain structures in certain regions to grow and be focused into preferred sectors while other perturbations decay. If similar calculations are performed, each from a different random initial condition, then more examples of preferred, time-evolving structures are produced. From a sufficient number of such integrations, what amounts to a climatology of the dominant, fast timescale disturbances of the model can be formed. This is the method we choose to find the geographical distribution and structure of fast timescale disturbances that should tend to be preferred in a linear model; that is, this is the technique we use to find the storm tracks for a given background state. It does not suffer from the shortcomings of the eigenvalue/eigenvector technique since it takes all modes into account; it weights the influence of each mode according to that mode's natural growth rate, frequency, and projectability; and the technique is not restricted to normal modes. The generation of transients from random initial perturbations may not match the situation in nature where certain types of cyclogenesis rely on the preexistence of perturbations with special structure (like the mobile upper-tropospheric troughs of type B cyclogenesis). However, the use of random perturbations means that the model's distribution of storms is completely determined by its background state, thus providing us with the information about the influence of the time mean state that we desire.

Since our goal is to understand the influence of patterns A and B on bandpass eddies in the GCM simulation used to define these patterns, the linear model employed in our study is a linearization of that GCM. This is the same linear model employed by Branstator (1990, 1992) to investigate the forcing anomalies that stimulate these patterns, though in the current study a version of the model with time-dependent rather than steady perturbations is used. It is based on the same (primitive) equations as the GCM and is discretized in space in the same manner though at reduced truncation: it uses five evenly spaced vertical levels, and its spherical harmonic basis is truncated at zonal wavenumber 10; for each zonal mode there are 16 complex meridional modes. Tests show little sensitivity of our results to the fact that the model uses fewer zonal modes than the GCM to which it is compared. Computing limitations have precluded testing the impact of using the coarsened vertical resolution, but results presented in succeeding paragraphs indicate the vertical structure of perturbations generated with five levels can be made to approximate the structure of perturbations in the GCM. The model contains no parameterization of physical processes except for Fickian dissipation with a coefficient of 2.5×10^5 m^2 s^{-1} (to match the GCM) and lowest layer Newtonian and Rayleigh terms. For reasons to be explained shortly, the timescale for both these terms is set to 2 days. Background states for the model are time-average fields from the GCM control run and are made symmetric with respect to the equator, though no such restriction is placed on the perturbations. Because the perturbations of primary interest in our study are located in midlatitudes and are of relatively small meridional extent, the use of a symmetric state has no important effect on our results. Time integration of the model equations is accomplished using an implicit scheme with a 2-hour time step. The model variables are sampled every 4 hours and the time average from each integration is removed as a simple means of isolating the transient component of the perturbation fields. Thirty integrations of the model, which together result in 60 hemispheric cases, are used to construct the collection of states that form the climatology of perturbations associated with a given background state.

The available free parameters in the problem are used to tune the storm tracks of the linear model to match the climatological storm tracks of the GCM that we are studying. The quantity that we use to characterize the storm tracks for this tuning process is the variance of 1–7 day bandpass 300-mb streamfunction. As shown in Fig. 3a, in the 200-month simulation used to construct patterns A and B, the GCM concentrates bandpass variance in two swaths across the Pacific and Atlantic rather like the storm tracks that occur in nature (Blackmon 1976). We choose parameters that produce a distribution of bandpass variance in the linear model that approximates Fig. 3a when the model is linearized about the 200-month Northern Hemisphere mean state from the GCM.

The most straightforward choice for the linear model has to do with the amplitude of the initial perturbations. We find that for the choice of other parameters to be discussed shortly, if the spherical harmonic coefficients for the initial perturbations are taken from a uniform

FIG. 1. Composite anomalies of quantities from a 200-month perpetual January simulation with an NCAR GCM. Composites are for those months for which the monthly mean 300-mb flow had a large projection onto either the second or third principal EOF of monthly mean 300-mb streamfunction. The 20 months with the largest positive projections are included. (a) The 300-mb streamfunction for months with large projections onto EOF2. This is referred to as pattern A in the text. Contour interval: 1.5×10^6 m^2 s^{-1}. (b) Same as (a) except for EOF3. This is pattern B. (c) Variance of 300-mb streamfunction with periods between 1 and 7 days for EOF2. Contour interval: 4×10^{12} m^4 s^{-2}. (d) Same as (c) except for EOF3. Contour interval: 4×10^{12} m^2 s^{-2}. (e) The 300-mb streamfunction tendency induced by 300-mb perturbations with periods between 1 and 7 days ($-\nabla^{-2}\mathbf{v}'_\psi \cdot \nabla\zeta'$) for EOF2. Contour interval: 4 m^2 s^{-2}. (f) Same as (e) except for EOF3. Contour interval: 2 m^2 s^{-2}. In this and succeeding figures, dashed contours are used for negative values and the zero contour is plotted with a dash–dotted line.

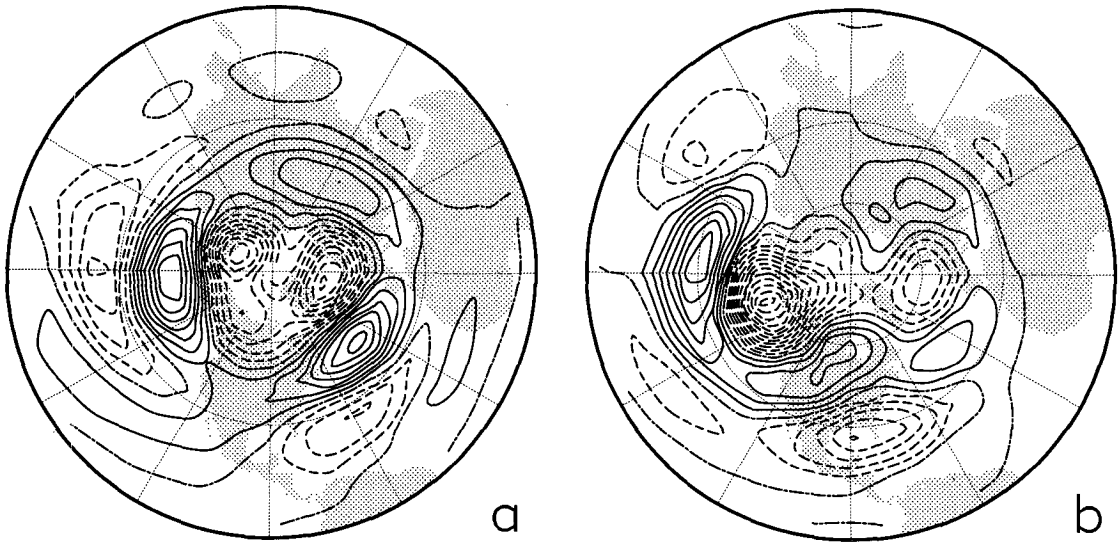

FIG. 2. Two common structures of streamfunction at $\sigma = .336$ in 200 steady solutions of a linear model forced by monthly mean anomalies of GCM vorticity fluxes from bandpass eddies. The two leading EOFs (LEOF1 and LEOF2) of these 200 solutions explain 30% and 26% of the variance, respectively. (a) LEOF1 + LEOF2. (b) LEOF1 − LEOF2.

distribution between −1.3 and 1.3 ($\times 10^{-6}$ s^{-1}) for vorticity, from a distribution between −1.3 and 1.3 ($\times 10^{-7}$ s^{-1}) for divergence, and from a distribution between −1.3 and 1.3 K for temperature, then the amplitude of the 300-mb bandpass variance constructed from integrations of the storm track model is similar to the bandpass variance from the GCM. Initial conditions with amplitudes set to these values are used in all experiments discussed in this paper.

A less obvious choice concerns the length of each integration used to collect the storm track statistics. One could reason that we need all stages of the life cycles of storms to affect our statistics, and since even in their most rapidly evolving cases Simmons and Hoskins (1978) found that it took about 10 days for a baroclinic disturbance to progress through a complete cycle, we should integrate our model for at least 10 days. However, when we choose 10 days for the integration length, the distribution of bandpass 300-mb streamfunction variance is not very similar to the distribution from the GCM. As seen in Fig. 3b, the variance is spread across one long storm track and has its maximum at the longitude where the GCM's bandpass variance is a minimum (Fig. 3a). The implication is that initial disturbances on the east coast of Asia grow as they move across the Pacific rather than begin to decay at the date line as they do in the GCM. One mechanism that has been proposed as an explanation for the decay of storms at the end of the storm tracks, namely, downscale cascade of bandpass energy to the dissipation range (Lee 1994) through the shearing effect of the time mean flow, is present in the linear model, but clearly it is not sufficient to terminate the Pacific storm track. The absence from the linear model of two other processes, namely, local reduction of the surface temperature gradient by the action of the eddies [as in the experiments of Simmons and Hoskins (1978)] and stabilization of the disturbances by the barotropic component of the growing perturbations [as in the barotropic governor mechanism studied by James and Gray (1986) and Nakamura (1993)], probably contributes to the lack of decay in the central Pacific. Plots (not shown) of the covariance of perturbation temperature and perturbation meridional wind at 700 mb in the GCM and in the linear model indicate that the generation of transient available potential energy occurs much farther into the eastern Pacific region in the linear model than in the GCM, suggesting that the absence of the first of these mechanisms is certainly playing a role in extending the Pacific storm track too far to the east in the linear model. As a simple means of parameterizing the decay stage of the life of a disturbance, we shorten the length of our integrations to 5 days. This means that disturbances that are initially in the strong baroclinic zones grow for about 5 days as they are advected through these zones, but they are not allowed to continue into regions that nonlinear decay processes normally prevent them from reaching. The distribution of bandpass 300-mb streamfunction variance for 30 integrations of the linear model of this duration (Fig. 3c) shows a much better match to the GCM storm track, including a local minimum between the Pacific and Atlantic storm tracks caused by the local minimum in baroclinity in the eastern Pacific. Given this similarity, 5-day integrations are used for experiments in the remainder of this work.

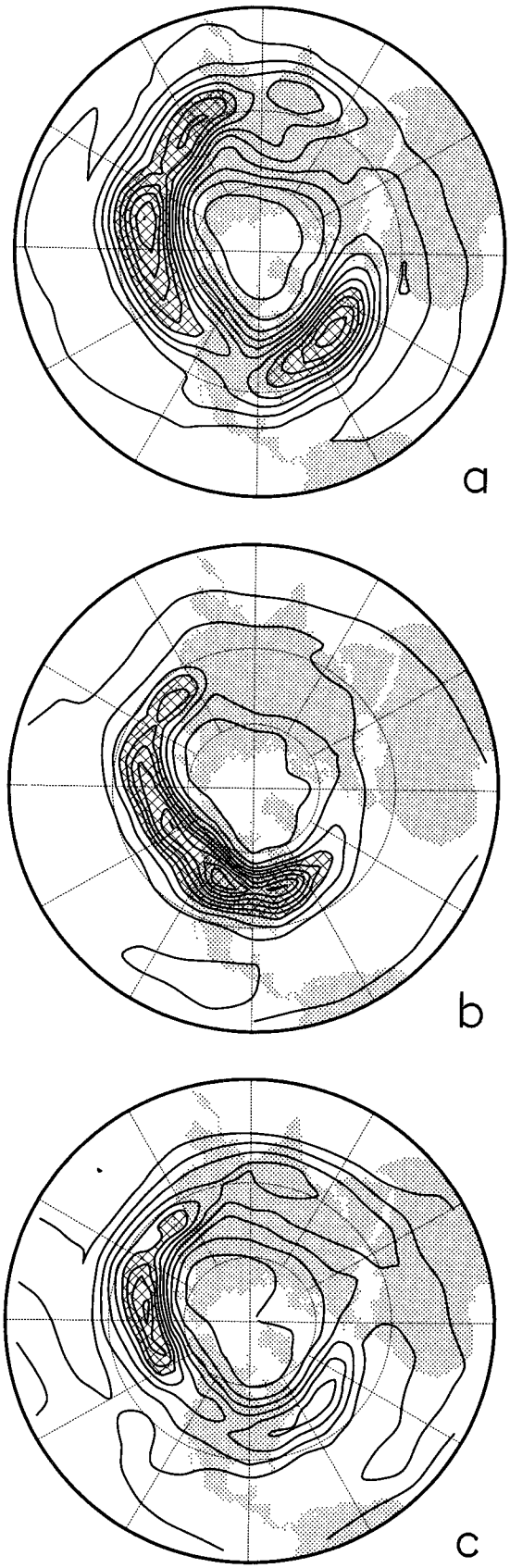

Newtonian and Rayleigh coefficients are the final parameters that must be chosen. Observational studies of bandpass transients, like that of Lau (1978), find a distinct maximum of kinetic energy in the upper troposphere. However, in baroclinic instability calculations with either zonally symmetric (like Simmons and Hoskins 1977) or zonally asymmetric basic states (like Frederiksen 1983), in addition to the upper-tropospheric maximum, there is one of approximately equal amplitude near the surface. Though Simmons and Hoskins (1977) attributed this discrepancy to the shortcomings of linear dynamics, Valdes and Hoskins (1988) have argued that Ekman pumping may be at least partially responsible for a weakening of the lower-level maximum in nature and found that a Rayleigh drag term in the lower portion of their linear model provided a good approximation to this Ekman effect. If our model is integrated 30 times for 5 days with no Rayleigh or Newtonian damping, then it has the double maximum noted in previous instability investigations. This is evident if we calculate the variance of bandpass streamfunction at each level and summarize the vertical structure of this variance by least-squares fitting a function to the vertical profiles of this variance at all model grid points between 20° and 70°N. The function drawn with a light solid curve in Fig. 4 is the result of such a fit. It explains about 96% of the gridpoint to gridpoint variance of the model profile and has two distinct maxima. A similar calculation for GCM bandpass streamfunction variance is drawn as the dotted curve in Fig. 4. This function explains about 99% of the variance but has only the upper-tropospheric maximum. If the linear calculation is redone with Newtonian and Rayleigh timescales of 2 days in the bottom layer, then the vertical profile drawn with a heavy line in Fig. 4 results. This profile explains 99% of the variance and is a much better match to the GCM's vertical structure than the profile produced with no bottom layer damping. Thus, we use a characteristic time of 2 days in the lowest layer as the standard damping in the linear storm track model. (This value was used for the calculations shown in Figs. 3b,c.) The choice of a 2-day timescale is not solely the result of picking a coefficient that fits the GCM variance profile; it is close to the value one finds for the average effective damping coefficient in the GCM simulation that results from bottom layer surface

FIG. 3. (a) Variance of 1–7 day bandpass 300-mb streamfunction for climatological conditions in the GCM simulation. Contour interval: 1×10^{13} m^4 s^{-2}. (b) Variance of transient 300-mb streamfunction in the storm track model linearized about the GCM Northern Hemisphere climate and integrated for 10-day segments. Contour interval: 4×10^{13} m^4 s^{-2}. (c) Same as (b) except integrations are 5-day segments. Contour interval: 1×10^{13} m^4 s^{-2}. Regions with values greater than 9×10^{13} m^4 s^{-2} are crosshatched in panels (a) and (c). Crosshatching begins at 16×10^{13} m^4 s^{-2} in panel (b).

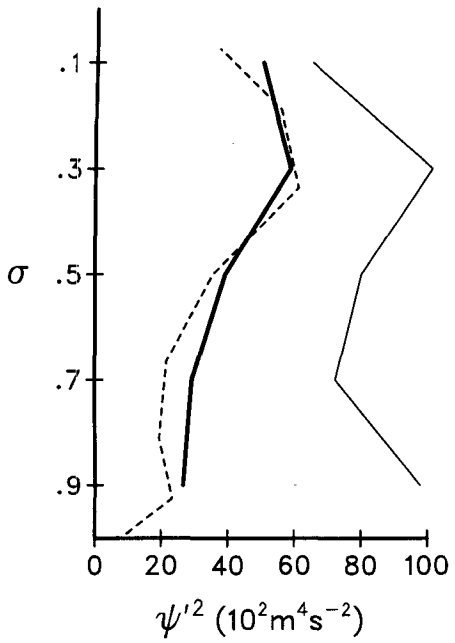

FIG. 4. Vertical profiles of bandpass (in GCM) or transient (in linear storm track model) streamfunction variance. As explained in the text, these lines show the leading EOF of profiles at model grid points between 20° and 70°N multiplied by one standard deviation of the projections onto the EOFs. Dashed: GCM. Heavy solid: storm track model with 2-day Rayleigh and Newtonian damping at lowest level. Light solid: storm track model without lowest-level damping.

stress. It is also similar to the value Valdes and Hoskins (1988) determined to be appropriate for their study.

b. *Momentum and heat flux verification*

Having developed a model that approximates the vertical and horizontal distribution of bandpass streamfunction variance for climatological GCM conditions, we will now check other, untuned, climatological fields to see how well they are reproduced in the linear model. We are especially interested in the momentum fluxes because they are instrumental in maintaining the two low-frequency patterns that motivated our study (Branstator 1992), and they have also been found to be more important than anomalous heat fluxes during episodes of teleconnection patterns in nature (Lau and Nath 1991). If our model does not reproduce these fluxes well for climatological conditions, then it will not be very useful for investigating momentum fluxes during anomalous low-frequency conditions.

For momentum fluxes in the linear storm track model to closely match those in the GCM, the amplitude and structure of bandpass eddies must be similar in the two models. As a means of quantifying these attributes, we calculate **E** vectors (Hoskins et al. 1983) from bandpass nondivergent 300-mb winds for both models. Among other things, the **E** vectors indicate the predominant shape of the eddies, as well as the effect they have on the mean flow as a result of momentum flux convergences. Figure 5a shows the **E** vectors for the GCM. The most prominent features are the high-amplitude vectors in the eastern sectors of the two storm tracks. Their generally zonal orientation indicates the eddies are meridionally elongated in these regions, and the fact that they diverge indicates that the transients are positively reinforcing the time mean in these regions, just as observational studies like those of Hoskins et al. (1983) and Lau and Holopainen (1984) have found. The tendencies induced by these eddies, as given by the inverse Laplacian of the divergence of the vorticity flux for bandpass nondivergent perturbations, are contoured on this same figure. Again, it is apparent that the eddies help to maintain the time-averaged westerlies in the eastern sectors of the storm tracks. Figure 5b depicts the same quantities for the linear model when the Northern Hemisphere climatology from the GCM is used as the basic state. Though the Atlantic **E** vectors are weak and the southern flank of both storm tracks does not extend far enough south, there is a great deal of similarity between this figure and Fig. 5a. Not only is the westerly acceleration in the storm track regions evident, but much weaker features throughout the midlatitudes and Tropics of the GCM climate are also present in the statistics of the linear storm track model.

Though not as important as momentum fluxes for the maintenance of low-frequency anomalies, heat fluxes are of such fundamental importance to the general circulation that it is of interest to check how well the linear model reproduces their distribution. In Fig. 6 are displayed the covariance between 700-mb temperature and the meridional component of the nondivergent wind for bandpass fields from the GCM and linear model. The GCM has the usual distribution with two main centers in the storm tracks. The linear model produces both of these features, but in keeping with the weak Atlantic storm track seen in terms of momentum, the Atlantic heat fluxes are dwarfed by the Pacific heat fluxes. Also, the Pacific fluxes are much too strong. This tendency for strong heat fluxes is also seen in Fig. 7, which shows vertical profiles of heat flux for the two models. As with streamfunction variance, these profiles are the result of fitting functions to heat fluxes that have been calculated at each model level in the band between 20° and 70°N. For both models this procedure leads to functions that represent about 92% of the gridpoint to gridpoint variance. The general profile from the linear model captures the vertical distribution found in the GCM, but as noted in linear modal studies (like Simmons and Hoskins 1977), when the linear results are scaled

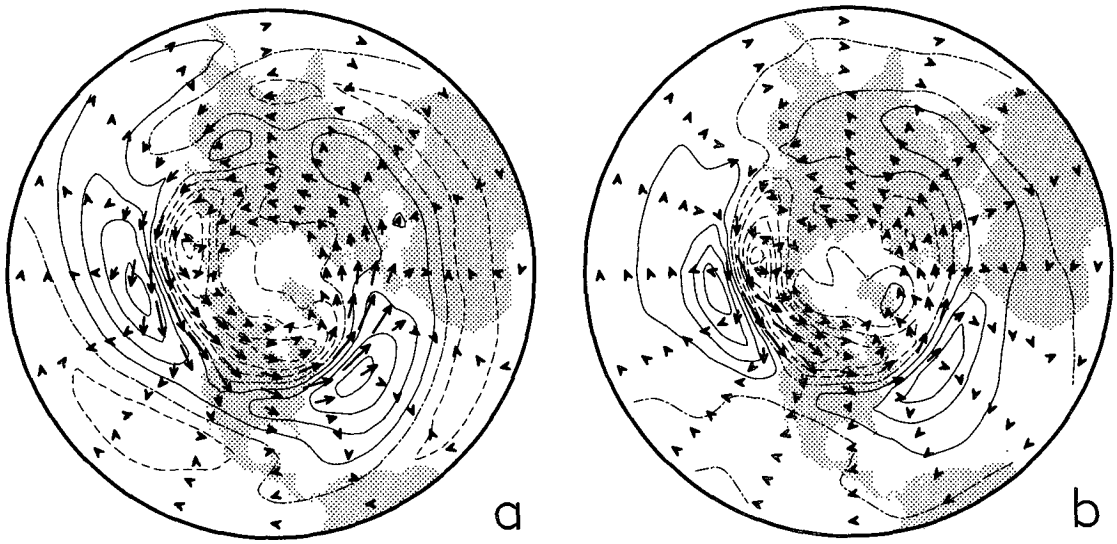

FIG. 5. The **E** vectors and contours of streamfunction tendency by vorticity fluxes ($-\nabla^{-2}\mathbf{v}'_\psi \cdot \nabla\zeta'$) for (a) 300-mb bandpass transients in the GCM and (b) 300-mb transients in the storm track model when linearized about the GCM climate. Contour interval: 6 m^2 s^{-2}. Scale of **E** vectors is the same in both panels.

so that momentum flux amplitudes match observed amplitudes the heat fluxes are too large.

c. *Verification with other basic states*

As a means of determining whether the linear storm track model is valid for states other than the Northern Hemisphere January GCM climate that was used in its tuning, we apply it to other long-lived states. One fairly extreme test of the robustness of the model is to test it with Southern Hemisphere January conditions from the same GCM simulation used to tune the storm track model. As documented by Pitcher et al. (1983), this GCM's Southern Hemisphere climate has marked deficiencies, but it does serve as a satisfactory testbed for checking the storm track model under conditions other than those to which it was tuned. The GCM storm track in terms of 300-mb bandpass streamfunction variance for the Southern Hemisphere is shown in Fig. 8a. Taking into account the different contour interval used in

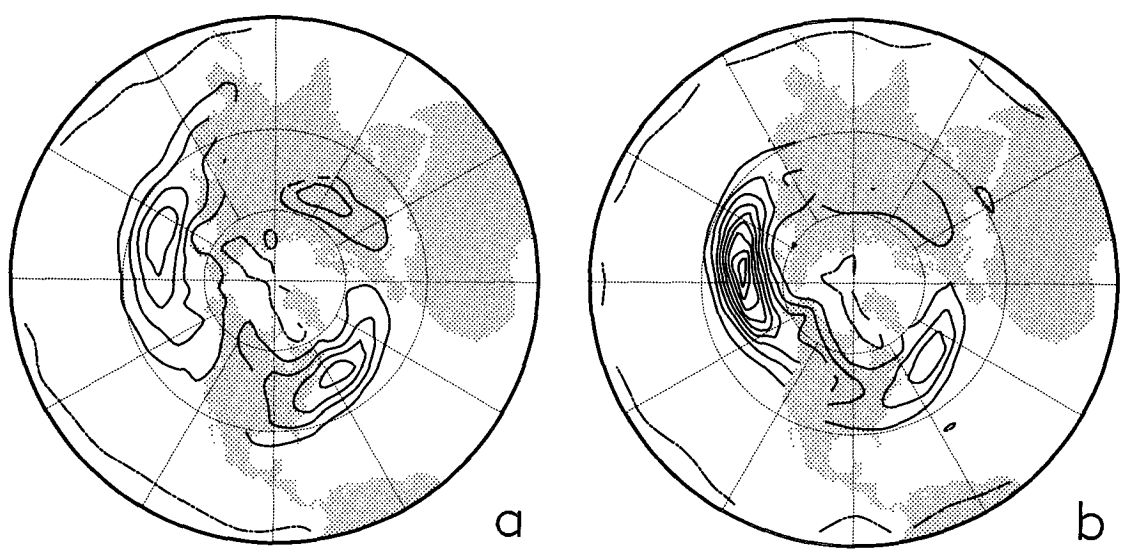

FIG. 6. (a) $\overline{v'T'}$ for bandpass 700-mb transients in the GCM. Contour interval: 10 m K s^{-1}. (b) $\overline{v'T'}$ at 700-mb for transients in the storm track model linearized about the GCM climate. Contour interval: 10 m K s^{-1}.

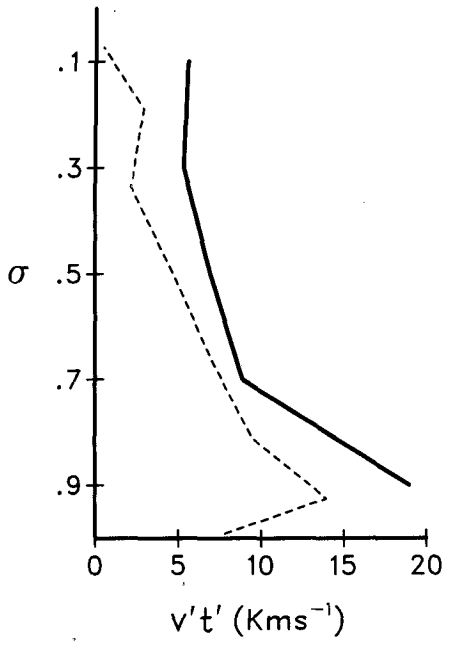

FIG. 7. Same as Fig. 4 except profiles are of $\overline{v'T'}$.

this plot, the most striking aspect of this plot is its small amplitude compared to the corresponding Northern Hemisphere chart (Fig. 3a). When linearized about the GCM Southern Hemisphere time mean state, the linear model reproduces the weak amplitude of Southern Hemisphere bandpass variance (Fig. 8b), as well as the general locations of the two midlatitude maxima in variance, though the Pacific track is too broad and too strong. Even the region of enhanced variance in the tropical Pacific that is evident in the GCM has a counterpart in the linear calculation.

Another test of the storm track model is to apply it to observed rather than simulated conditions. To do this we calculate the variance of Northern Hemisphere 1–7 day bandpass 300-mb streamfunction analyzed by the European Centre for Medium-Range Weather Forecasts for December, January, and February during the winters of 1980/81 through 1990/91. Shown in Fig. 8c, the variance in this data is generally broader than that for the GCM, has a Pacific storm track that extends much farther south to the east of the date line than that in the GCM, and has an Atlantic storm track that reaches farther into Europe than does the corresponding track in the GCM. When linearized about the time mean state from the same 11 winters, the linear storm track model produces the 300-mb bandpass streamfunction variance depicted in Fig. 8d. Though probably not as good a match as its approximation of the GCM's Northern Hemisphere storm track, this solution by the linear model does capture most of the important features of the observed storm track. In particular, it reproduces each of the three characteristics that distinguished the observed storm track from the GCM simulated storm track. Perhaps the most noticeable weakness of the distribution in Fig. 8d is the local maximum stretching across Africa and southern Asia that is not present in the observations. This feature occurs at higher altitudes in the observations; its presence in the linear model at 300 mb may be a reflection of that model's coarse vertical resolution. It may also be more prominent in the storm track model because that model does not include the effects of enhanced surface stresses and reduced latent heat release that can decrease the strength of disturbances over land compared to disturbances over oceans.

3. Application to low-frequency anomalies

The linear storm track model described in section 2 appears to have the attributes that we need to determine what effect low-frequency anomalies have on the distribution and structure of storms. For a given climate it can produce a good approximation to the storm track statistics for that climate based on nothing but the time mean flow. It does this assuming no feedbacks of the transients onto the time mean state so that it is clear that the configuration of the time mean causes the storm track structure, and it has been found to be valid for states that are quite different from the state used in its tuning. We now use it to determine the storm tracks that would be expected to occur as a result of prominent perturbations in the control climate of the GCM, namely, patterns A and B. The amplitude of these perturbations is small compared to the range of climates that were used in section 2c to validate the linear storm track model, so it is reasonable to use it to find the storm tracks expected to result from the presence of these anomalies in the quasi-stationary component of the flow. Patterns A and B are composites of monthly mean data, so the states we are now considering may have timescales that are considerably shorter than the time mean states used in the tests of section 2c, but since their timescale is long compared to the lifetime of storms, the use of the linear model to determine the influence of the anomalies on storm tracks is valid.

To find the influence of pattern A, we form a basic state consisting of the time-averaged flow from the GCM Northern Hemisphere perpetual January experiment during those days that contribute to the composite of Fig. 1a. Using the same procedure and model parameters employed in the climate tests, bandpass statistics for the linear model with this new basic state are calculated. The difference between these statistics and the statistics from the storm track model linearized about the GCM standard Northern Hemisphere climate indicates the anomalies in storm track structure that are caused by the presence of pattern A. For example, the difference in 300-mb bandpass streamfunction variance

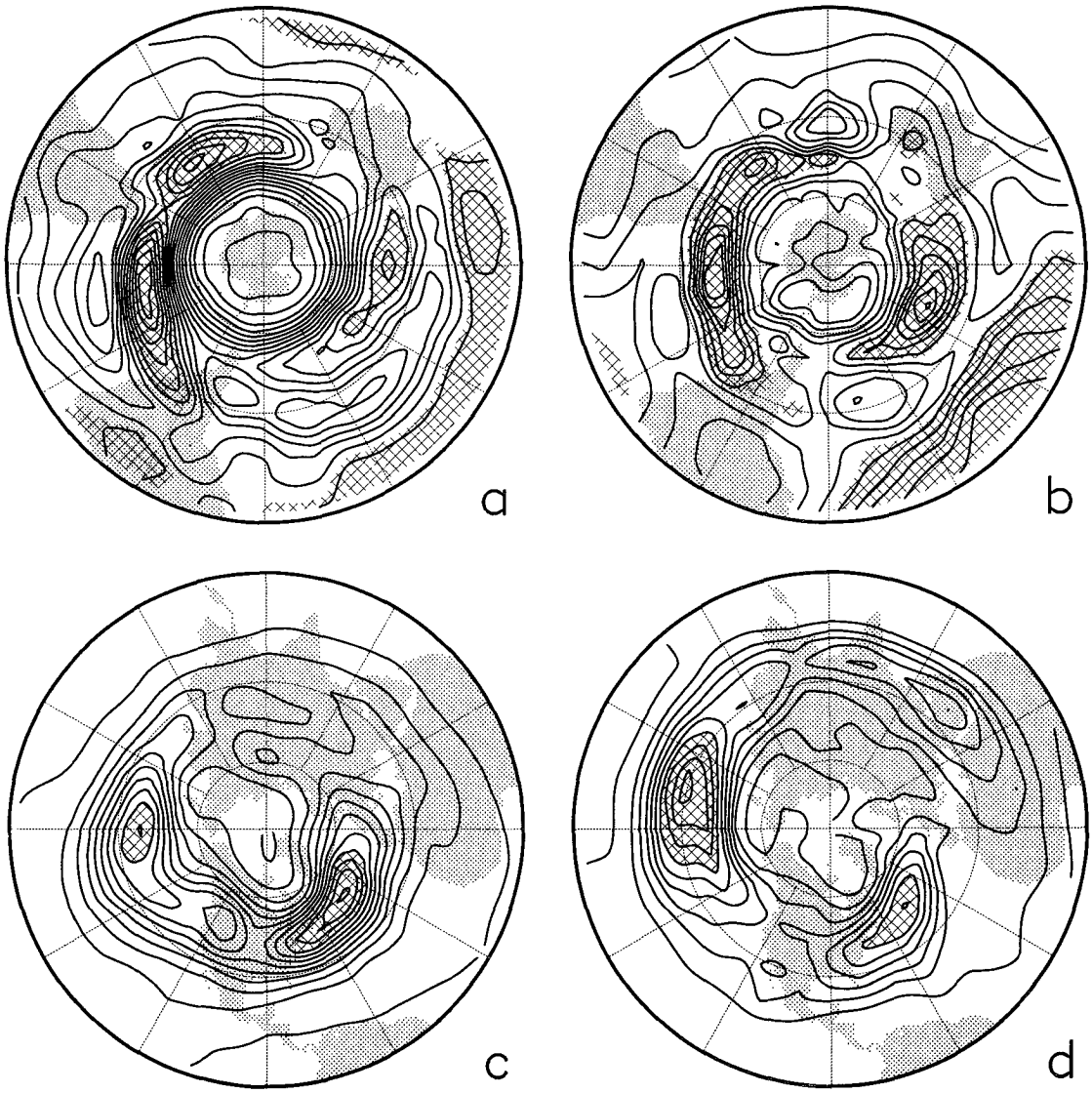

FIG. 8. (a) Variance of bandpass 300-mb streamfunction for the Southern Hemisphere in the GCM. Contour interval: 3×10^{12} m^4 s^{-2}. (b) Variance of 300-mb transient streamfunction in the storm track model linearized about the GCM Southern Hemisphere climate. Contour interval: 3×10^{12} m^4 s^{-2}. (c) Same as (a) except for observed Northern Hemisphere December, January, and February observations. Contour interval: 1×10^{13} m^4 s^{-2}. (d) Same as (b) except model is linearized about observed Northern Hemisphere December, January, and February climate. Contour interval: 1×10^{13} m^4 s^{-2}.

(Fig. 9a), when compared with the 300-mb bandpass streamfunction variance from the storm track model linearized about the standard climate state (Fig. 3c), shows that the effect of pattern A is to produce a northeastward shift in the Pacific storm track and a northward shift in the Atlantic storm track. This is the same redistribution of bandpass activity that occurs during episodes of pattern A in the GCM (Fig. 1c), so we conclude that in the GCM the anomaly in bandpass variance is caused by the presence of pattern A. For the issue of low-frequency maintenance, it is more important to understand what causes anomalies in momentum flux convergence than to determine the cause of anomalies in variance. But if we plot the anomalous 300-mb streamfunction tendency from momentum fluxes by bandpass eddies (Fig. 9c), we see that we come to the same conclusion. The storm track model indicates that the influence of pattern A is to shift the climatological forcing by the bandpass momentum fluxes (Fig. 5b) to the north over the Western Hemisphere, which is the same effect that anomalous bandpass eddies have when pattern A is present (Fig. 1e).

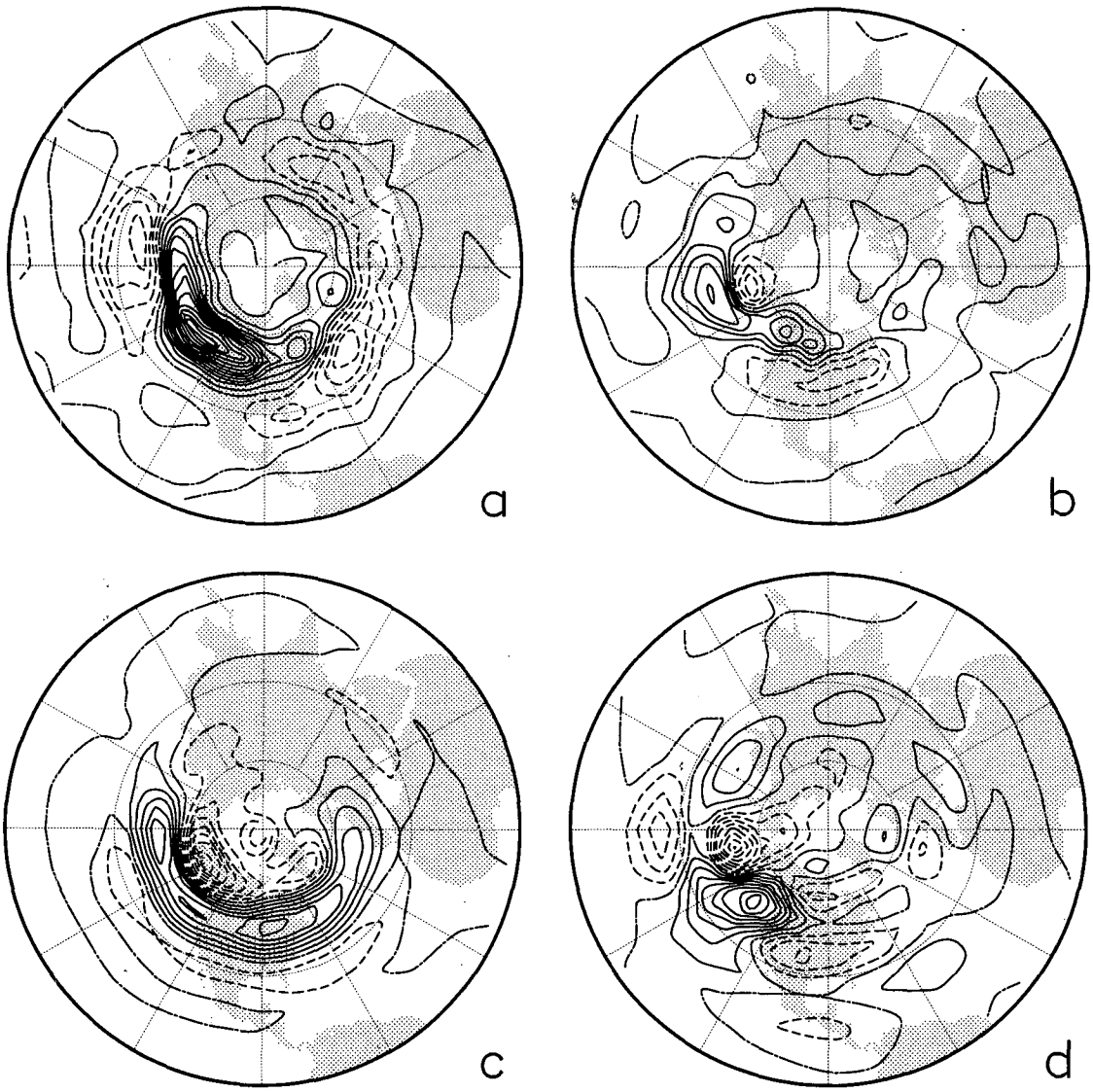

FIG. 9. (a) Variance of transient 300-mb streamfunction when pattern A is added to the climatological flow to form the basic state minus this variance when pattern A is not included in the basic state, as given by the storm track model. Contour interval: 4×10^{12} m^4 s^{-2}. (b) Same as (a) for pattern B. Contour interval: 4×10^{12} m^2 s^{-2}. (c) Same as (a) except quantity is anomalous streamfunction tendency induced by vorticity fluxes $(-\nabla^{-2}\mathbf{v}'_\psi \cdot \nabla\zeta')$. Contour interval: 4 m^2 s^{-2}. (d) Same as (c) except for pattern B. Contour interval: 2 m^2 s^{-2}.

The linear storm track model also indicates that the major storm track anomalies that coincide with the occurrence of pattern B are caused by pattern B. This can be seen in Figs. 9b and 9d, which show the anomalous 300-mb bandpass streamfunction variance and streamfunction tendencies from bandpass momentum fluxes that result in the linear model when its basic state is the time mean GCM flow during episodes of pattern B. The structure of the strongest features in both these fields is similar to the corresponding quantities, shown in Figs. 1d and 1f, that occur in the GCM when pattern B is prominent.

4. Mechanisms

Having used the linear storm track model to determine that the presence of low-frequency perturbations helps to organize low-frequency anomalies in bandpass activity, we now wish to understand which mechanisms are instrumental in bringing about this organization. One fundamental issue is whether the persistent anomalies act by changing the position and strength of the baroclinic zones, whether their primary effect is to change the principal routes taken by storms through modification of the steering winds, or whether they act

to change the structure of individual storms through stretching and straining. As a first step toward addressing this question, we calculate the storm tracks that would occur if patterns A and B were strictly barotropic by linearizing the storm track model around states consisting of the standard GCM climate mean plus the vertically averaged wind anomalies from the patterns. A surface pressure anomaly is also added to bring the basic state into near geostrophic balance. Figures 10a and 10b show the anomalous bandpass streamfunction variance that is induced by these barotropic renditions of patterns A and B. Though amplitudes of individual features are somewhat different in the barotropic experiment for pattern B than they were when the complete version was used (Fig. 9b), all of the main anomalies are produced. The similarity between the barotropic experiment and the calculation with a complete version of pattern A (Fig. 9a) is not as great. All of the important anomalies are present in the simplified situation, but for most features the barotropically produced anomalies are weak, especially over northern North America. If we use streamfunction tendency rather than variance as our measure of storm track anomalies, then the importance of the barotropic component is more obvious. Tendency anomalies for barotropic patterns A and B (Figs. 10c and 10d) are quite good approximations to the tendency anomalies that resulted in the storm track model when unaltered patterns A and B were added to the basic state (Figs. 9c and 9d).

Given the importance of the barotropic effect of patterns A and B, we employ a second means of analyzing its influence. This entails using the ray tracing equations employed by Karoly (1983) in his study of energy propagation through a zonally varying medium. As explained in that paper, for the linear nondivergent barotropic vorticity equation, the group velocity is given by the expressions

$$u_g = \bar{u}_m + [(k^2 + l^2)\bar{q}_y - 2kl\bar{q}_x]/K^4 \qquad (1)$$

and

$$v_g = \bar{v}_m + [2kl\bar{q}_y + (k^2 + l^2)\bar{q}_x]/K^4, \qquad (2)$$

where k and l are local zonal and meridional wavenumbers, respectively, $\bar{q}$ is basic-state absolute vorticity, $\bar{u}_m$ and $\bar{v}_m$ are the zonal and meridional basic-state wind components divided by cosine latitude, x and y are Mercator coordinates, and $K^2 = (k^2 + l^2)$. Following the group velocity, the central wavenumbers of wave packets evolve according to the relationships

$$\frac{d_g}{dt}k = -k\bar{u}_{mx} - l\bar{v}_{mx} + (k\bar{q}_{xy} - l\bar{q}_{xx})/K^2 \qquad (3)$$

and

$$\frac{d_g}{dt}l = -k\bar{u}_{my} - l\bar{v}_{my} + (k\bar{q}_{yy} - l\bar{q}_{xy})/K^2. \qquad (4)$$

To determine the effect of the barotropic component of the basic states used in our storm track calculations on the movement of wave packets that have formed in the storm tracks through baroclinic growth, we integrate (1)–(4) forward in time using values from the basic state at $\sigma = .300$ for $\bar{u}_m$, $\bar{v}_m$, and $\bar{q}$. We begin each integration with a disturbance just upstream of the region we are interested in and assign it initial values of $k = 8$ and $l = 0$. These values are selected because instability calculations with the storm track model when it is linearized about the various basic states in our study show the fastest growing modes tend to be predominantly composed of zonal wavenumber 8 and meridional wavenumbers between -2 and 2, depending on latitude. Our results are insensitive to the exact choice of meridional wavenumber. For example, to see where wave packets would tend to move in the eastern portion of the Pacific storm track solely from the barotropic influence of the upper-tropospheric standard climate winds, we consider packets at 170°E for various latitudes between 25° and 60°N and follow their progression for 2 days according to the ray-tracing equations. The straight dashed line at 170°E in Fig. 11a indicates the initial positions of this set of packets, and the dashed lines immediately to its east show the positions of the packets every 6 hours of the integration. These can be thought of as wave fronts. Also depicted on Fig. 11a is the evolution of a second wave front, one initiated with packets at 50°W in the Atlantic storm track. In both cases we can see the latitudinal dependence of the group velocity caused by horizontal shear in the background winds (shown in terms of streamfunction contours on the chart) and the tendency for wave activity on the southern flank of the jet to propagate into the Tropics, a phenomenon the **E** vectors of Fig. 5 imply occurs in the GCM and in the linear model's storm tracks.

In a similar fashion we calculate the evolution of wave packets under the barotropic influence of a basic state composed of the pattern A composite. This is shown in Fig. 11b. For both the Pacific and Atlantic sectors, it is apparent that the effect of pattern A is to cause high-latitude packets to move eastward more rapidly and midlatitude propagation to be retarded. If we think of the regions to the west of the initial wave fronts as being the primary sources of storm energy because of the strong background thermal gradients in those regions, then the effect of pattern A will be to enhance the strength of bandpass disturbances in high latitudes and weaken it in midlatitudes. From Figs. 9a and 10a, we recall that this is exactly the effect of pattern A in the storm track model. A second pair of ray-path calculations (not shown), this time employing basic states from the control and pattern B composites, gives similar results: changes in the distribution of bandpass variance caused by the presence of the barotropic com-

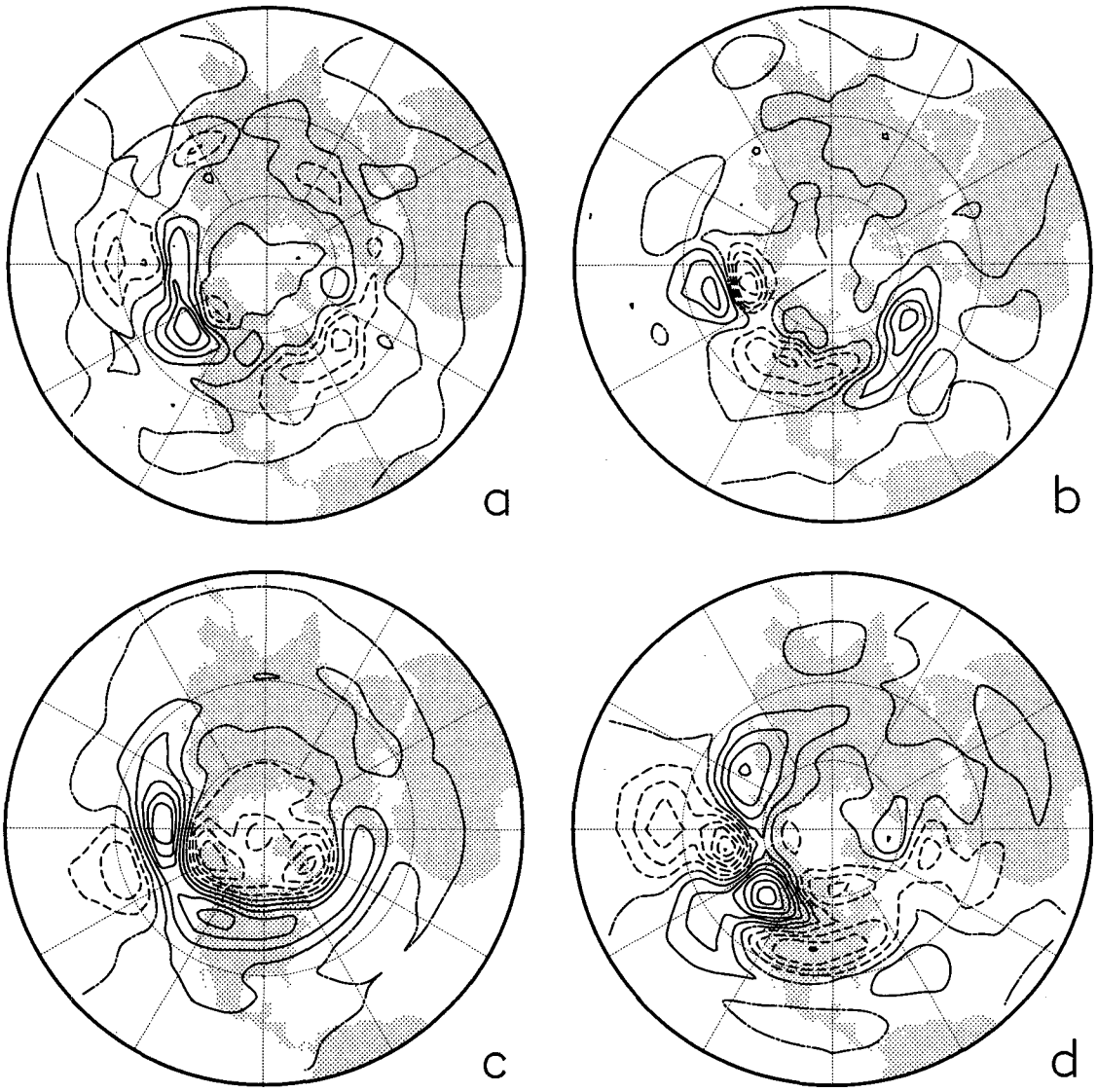

FIG. 10. Same as Fig. 9 except only the barotropic component of pattern A and B influence the calculation. Contour interval for (a) and (b) is 4×10^{12} m^4 s^{-2}, for (c) 4 m^2 s^{-2}, and for (d) 2 m^2 s^{-2}.

ponent of pattern B are reproduced by the ray-path method.

By modifying the ray calculation, the means by which barotropic patterns A and B influence the storm tracks can be identified more precisely. We mentioned that the advective effect of the jet on the evolving wave fronts was quite apparent in the bowed shape that they attained. If we modify Eqs. (1) and (2) so that group velocity is simply equal to the background velocity, then we can isolate this effect on storm migration. In Fig. 11c is the evolution of wave packet position under the influence of the standard climate when group velocity is approximated in this manner. The behavior is somewhat different than when the complete definition of group velocity is used (Fig. 11a), but the general character of the two sets of solutions reflects the same behavior. The same can be said when the approximate definition is used for a calculation of ray paths in the presence of pattern A (Fig. 11d). What is interesting for our purposes is that even with the simplified definition, the ray path calculation can be used to explain the shift in bandpass variance caused by the barotropic component of pattern A. Comparing Fig. 11d to Fig. 11c, in both the Pacific and Atlantic sectors eastward propagation is stronger at high latitudes and weaker at midlatitudes under the influence of pattern A. The simplified definition of group velocity works equally well at reproducing the influence of pattern B. Hence, the

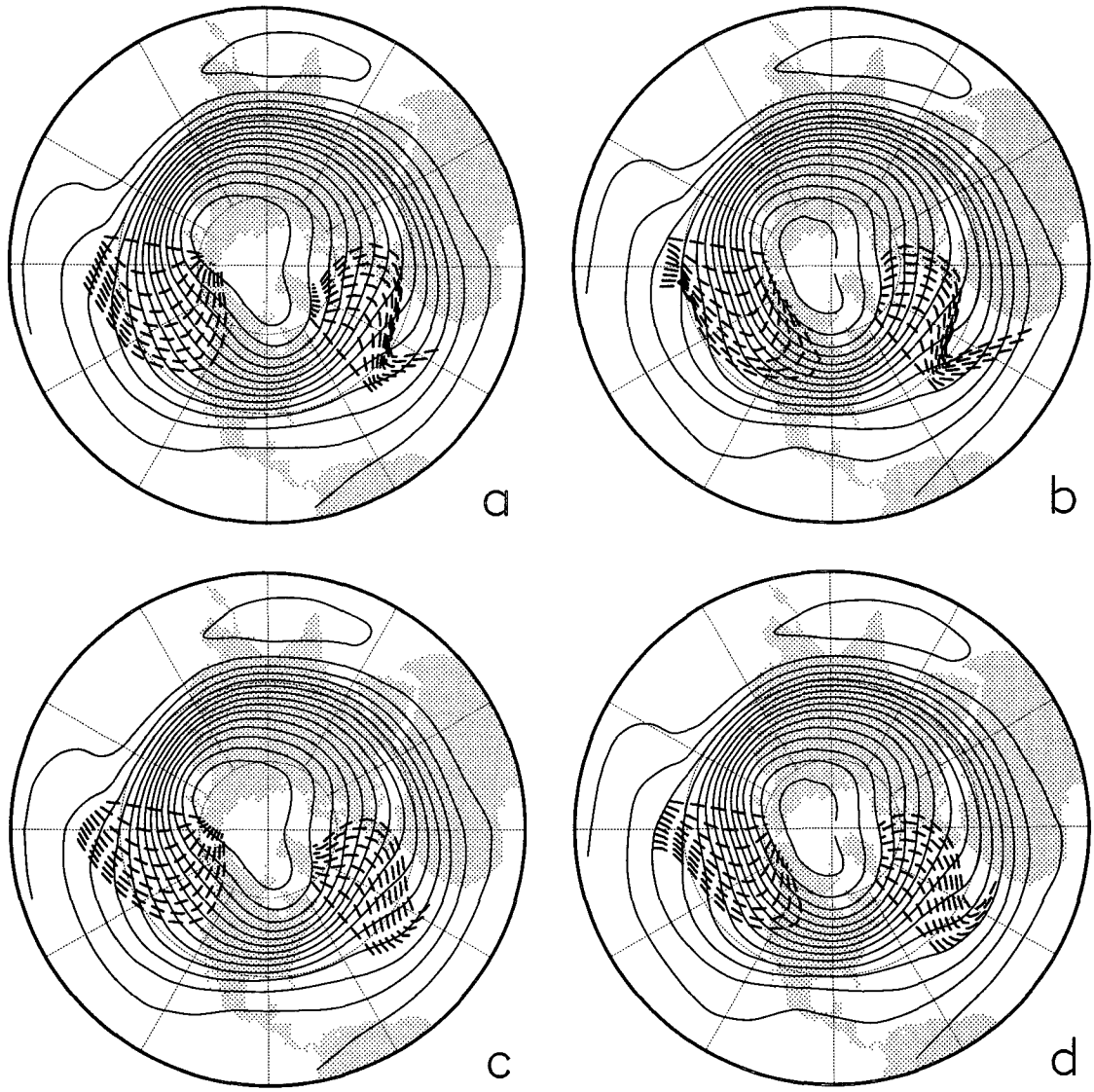

FIG. 11. (a) Dashed lines: wave fronts every 6 h for wave packets starting at 170°E and 50°W as determined from (1)–(4) for the climatological GCM state. Contours are of GCM climatological 300-mb streamfunction. Contour interval: 1×10^7 m^2 s^{-1}. (b) Same as (a) for wave packets in the mean flow on those GCM days included in the pattern A composite. (c) Same as (a) except group velocity set equal to climatological velocity. (d) Same as (b) except group velocity set equal to climatological velocity.

steering effect of the background anomalies, and not their stretching and straining and the modification to dispersion that would result, is sufficient to qualitatively explain the bandpass variance anomalies caused by the barotropic low-frequency anomalies. However, this does not rule out the possibility that stretching and straining by the anomalies may account for anomalous fluxes by the transients through their effect on eddy tilts.

These results focus on attributes of the low-frequency anomalies. It is of equal interest to consider how important the configuration of the basic climate is in determining the impact that persistent anomalies have on storm track anomalies. To address this question, we consider the effect of patterns A and B in climates that differ from our control configuration. For example, we can ask whether zonal asymmetries in the climatological flow and the accompanying nonuniform distribution of bandpass disturbances are important to the formation of storm track anomalies by the low-frequency patterns. Using the storm track model, this question is addressed by calculating the storms that re-

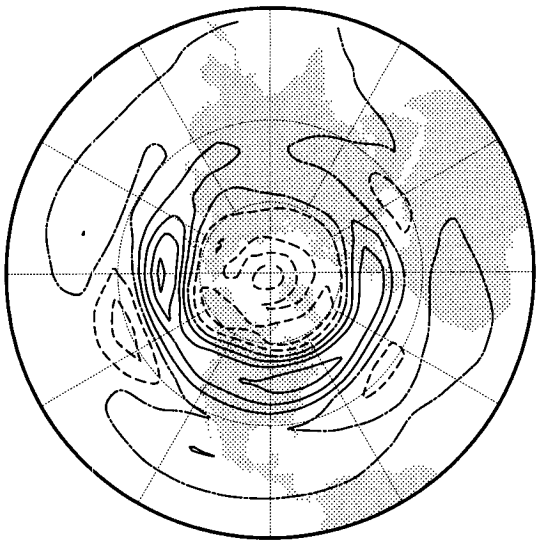

FIG. 12. Anomalous streamfunction tendency at 300 mb from vorticity fluxes for pattern A as calculated by the storm track model assuming a zonally symmetric climatology. Contour interval: 4 $m^2 s^{-2}$.

sult when the model is linearized about states consisting of zonal mean Northern Hemisphere climatological conditions from the GCM January simulation and comparing them to the storms that occur in the linear model when pattern A is added to this zonally symmetric background flow. It turns out that the bandpass statistics are not very stable when the storm track model is used in this way, probably because the eigenspectrum is not as peaked, so 200 rather than the usual 30 integrations must be performed. The anomalous 300-mb streamfunction tendency caused by pattern A in this experiment, as shown in Fig. 12, has a structure like that in Fig. 9c, which is the corresponding anomalous tendency field for a three-dimensional climate state. A second related experiment (not shown) in which pattern B is used to perturb the zonal mean GCM climate leads to the same result; the storm track anomaly in this situation is quite similar to the anomaly with a full climate basic state.

From the previous experiment one might conclude that the stationary waves in the climatological state are not an all-important factor, but further tests do not support this conclusion. If the pattern A composite anomaly is translated 90° to the east and added to the standard GCM climate and storms are calculated for this new basic state, then the resulting anomalous 300-mb streamfunction tendency is that displayed in Fig. 13a. This experiment can be interpreted as the addition of pattern A to a new climate, namely, the standard climate translated 90° westward. Under that interpretation if the climatological waves were unimportant, then Fig. 13a, when translated 90° westward, would match Fig. 9c, but it does not. Figure 13b is the anomalous tendency from a similar experiment, namely, one in which the pattern A composite is translated 90° westward and added to the standard climate. In this case, if the climatological waves were unimportant to the effect of pattern A, then Fig. 13b, translated 90° eastward, would be the same as Fig. 9c. In both of these cases, the pattern of anomalous tendencies does not shift as much as the imposed shift in the basic-state anomalies. This is probably explained by the fact that when translated to the east, the eastern portion of pattern A affects the

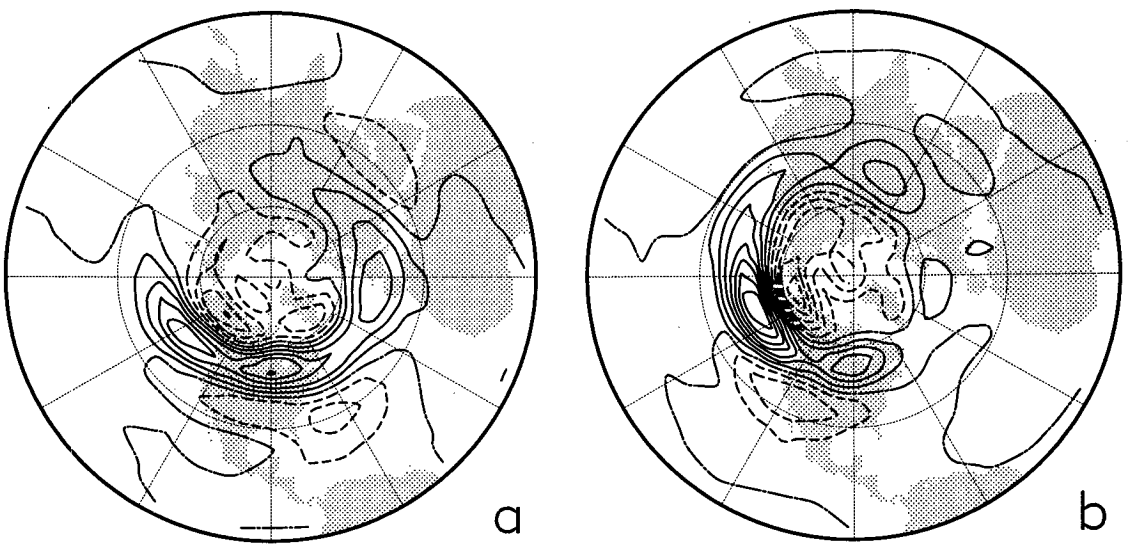

FIG. 13. Anomalous streamfunction tendency at 300 mb from vorticity fluxes calculated by the storm track model for pattern A when it is translated (a) 90° to the east and (b) 90° to the west. Contour interval: 4 $m^2 s^{-2}$.

region over Asia where there is little bandpass variance, and when translated to the west, its western portion is also over this minimum in storm activity. Thus, from these experiments one concludes an important property of the climatological state is that it simply provides bandpass disturbances for the low-frequency anomalies to redistribute. In its normal position, pattern A has its strongest lobes in regions where the climatological state provides a great deal of bandpass activity. The zonal mean climate also has bandpass variance in these regions, and therefore the effect of pattern A in that climate is essentially the same as in the standard climate.

5. Summary, discussion, and conclusions

Our study was motivated by a need to provide a rationale for the observed organization of anomalous storm track conditions. Anomalies in bandpass variance and in momentum fluxes by bandpass disturbances tend to have preferred structures, and in the GCM simulation used as the basis for our study, our calculations indicate that without these preferred structures the observed family of low-frequency flow anomalies would not be maintained. Based on the suggestive results of earlier studies, we hypothesized that the presence of preferred low-frequency flow anomalies in the GCM serve to bring about the storm track organization. This could happen through changes in the position and intensity of the baroclinic zones or by changes in the barotropic structure of the time mean winds resulting in the steering of storms to new regions or leading to changes in storm structure through the stretching and straining of their circulations.

To verify this hypothesis, a model was developed that could be used to generate the statistics of bandpass disturbances that would be expected to occur as a result of a given time-independent state. Because this model is linear and does not include the feedback of the bandpass perturbations onto the time mean, it could be used to unambiguously find the influence of low-frequency anomalies on bandpass disturbances. Having been tuned to approximate the bandpass variance statistics of an extended GCM control integration, the model was tested by comparing other aspects of its bandpass statistics, like momentum and thermal fluxes, with corresponding aspects of the GCM. Further verification of the model consisted of applying it to other climate states to make sure that the tuning procedure had not been too restrictive. In general, our simple model of the storm tracks proved to be even more successful at reproducing the storm track statistics of known climates than might have been expected from previous studies. In particular, nonlinear baroclinic life cycle studies, like that of Simmons and Hoskins (1978), have found that though momentum fluxes by the eddies are present during the initial linear growth of a disturbance, it is not until the nonlinear decay stage that these fluxes become significant. The presence of momentum fluxes that are too weak compared to thermal fluxes and the absence of an eastern Pacific decay region in the linear storm track model are consistent with the contention that nonlinearity is needed to produce complete life cycles. But our results do indicate that to a large degree the horizontal structures that lead to momentum fluxes can be generated by linear mechanisms. It is possible that these structures are better produced in our linear model than in some previous linear calculations because of the use of a zonally varying basic state (which might incorporate some of the effects of nonlinearity in the time mean state) and the use of structures other than fastest-growing modes for initial conditions.

Having confirmed that the storm track model could generate the bandpass statistics associated with a range of different climates, we then used it to determine the storm track anomalies that are induced by two patterns of low-frequency anomalies that often occur in the GCM. We found that, in terms of bandpass variance and streamfunction tendency from the bandpass transients, the storm track anomalies caused by the low-frequency anomalies were very similar to the storm track anomalies that coincide with and maintain the low-frequency anomalies, thus substantiating our study's hypothesis. We then performed additional experiments that indicated the importance of the barotropic component of the low-frequency anomalies in producing the storm track changes. The barotropic component was especially instrumental in bringing about the observed anomalous tendencies, which we know help maintain low-frequency anomalies. Furthermore, ray-tracing results suggest that to a certain degree the influence of the barotropic component can be understood in terms of its steering effect on the bandpass eddies.

Strictly speaking, our finding that low-frequency anomalies cause the storm track anomalies that are observed to occur simultaneously with them has only been demonstrated for two anomaly patterns, namely, the patterns we referred to as A and B. In fact, this result is more generally valid. For example, further experiments with the storm track model show that the storm track anomalies associated with episodes of patterns A and B when their sign is changed are also caused by those low-frequency patterns. Another example is the storm track anomalies that are observed to coincide with anomalies in individual Rossby–Haurwitz waves. Cai and Van den Dool (1991) have found that in nature storm track anomalies tend to follow the movement of individual large-scale waves. Simplifying their approach by considering different quasi-stationary phases of a single Rossby–Haurwitz wave rather than traveling waves, we find that a similar association between large-scale waves and storm tracks occurs in our GCM. One of the large-scale waves that Cai and Van den Dool investigated was similar to spherical har-

monic Y_6^1 in streamfunction; this is the one we now concentrate on. To obtain reliable statistics concerning the storm track anomalies associated with perturbations of Y_6^1 in the GCM, we make composites from eighteen 100-month perpetual January simulations. We composite the 300-mb streamfunction from those months from the simulations with largest projections onto one phase of Y_6^1 to arrive at a mean anomaly whose projection is equal to 6×10^5 m^2 s^{-1}. A mean anomaly with this amplitude is chosen because the standard deviation of projections onto any one phase of Y_6^1 is about this large. Such anomalies are produced for eight different phases of Y_6^1, each separated by 45°. The resulting mean anomaly fields consist predominantly of Y_6^1, though other components are present because spherical harmonics do not vary independently from each other. An example is the streamfunction anomaly of Fig. 14a that results when Y_6^1 has a phase that places antinodes at 90°E and 90°W. To find that bandpass variance associated with a particular phase of Y_6^1, we composite bandpass 300-mb streamfunction variance for the same months. For example, when this is done for those months used to produce Fig. 14a, the anomaly in bandpass variance shown in Fig. 14b results. The strongest features in this field are over North America, the same region where the monthly mean streamfunction anomalies are most pronounced. If the 300-mb streamfunction tendency caused by bandpass momentum fluxes is used as the indicator of the storm track, then we find that the pattern of Fig. 14d is the storm track change associated with the flow anomaly of Fig. 14a. From this example, as well as others not shown, it is apparent that there is a distinct relationship between the phase of Y_6^1 and the structure of the storm track in the GCM. To verify this relationship is present because the low-frequency anomalies are causing the observed anomalies in the storm track, we again use the storm track model, this time linearizing it about the GCM climate plus composite anomalies based on Y_6^1 projections. For the case of Fig. 14a, the storm track model indicates that the low-frequency anomaly would produce the variance and tendency anomalies of Figs. 14c and 14e, respectively. For both variance and tendency, every feature in the GCM composites is present in the storm track model's solution. When other phases of Y_6^1 are used as a compositing index, a similar conclusion is drawn: storm track anomalies associated with individual Rossby–Haurwitz waves are caused by the Rossby–Haurwitz wave anomaly.

The two low-frequency anomalies, patterns A and B, that our study has primarily dealt with were also examined by Branstator (1992). That study found that the same momentum flux anomalies that we have shown to be caused by these patterns make a major contribution to the maintenance of these patterns. Taken together, the two studies then are showing a two-way interaction by which anomalies in the two time-scales act to maintain each other. Thus, one could argue that a description of one of these patterns without mention of the storm track anomalies that accompany it is as incomplete as describing one of the patterns in terms of only one or two of its lobes. This is probably equally true for the long-lived anomalies of individual Rossby–Haurwitz waves considered in the previous paragraph, since comparison of the low-frequency anomaly in Fig. 14a with the tendency anomaly that is caused by it (Fig. 14e) suggests that those anomalous tendencies would tend to support the low-frequency anomaly.

The strong linkage between low- and high-frequency anomalies has a positive implication for extended-range forecasting. The maintenance of the low frequencies strongly depends on the statistics of the high frequencies. Since our study has shown these statistics to be largely controlled by the low-frequency anomalies themselves, prediction of long-lasting anomalies need not be limited by the predictability of individual high-frequency events.

The fact that many of the low-frequency anomalies we have considered in this paper, including individual large-scale Rossby–Haurwitz waves as well as patterns A and B, have the property that their effect on the bandpass eddies leads to a positive feedback naturally leads to the question: Do all large-scale anomalies induce a positive feedback? This is a topic that needs further investigation, but based on the calculations of section 4, the answer would seem to be no. Results from that section indicated that a translated pattern A would not induce a positive feedback, perhaps because the translated pattern did not intersect the climatological storm tracks over much of its extent. If the answer is no, then this raises the possibility that those patterns that do produce a positive feedback have a natural advantage over those that do not. Hence, the presence or absence of a positive feedback could be a means of natural selection that determines which flow anomalies preferentially occur in our GCM and in nature. That we have found a positive feedback for all patterns that actually occur in the GCM and did not find a strong feedback for those patterns that were artificially introduced into the storm track model (namely, translated pattern A) seems to support this possibility.

Though developed for diagnostic purposes, the storm track model used in this study may prove useful as a means of parameterizing small-scale transients in certain applications. Our results indicate that it could be especially useful in situations where the statistics of momentum fluxes by bandpass transients are needed. That these fluxes are largely determined by the barotropic component of low-frequency anomalies could greatly simplify such a parameterization. We have not tested the model's ability to generate the heat fluxes that are caused by flow anomalies, but its success at approximating the geographical distribution of heat fluxes associated with a climatological mean flow in-

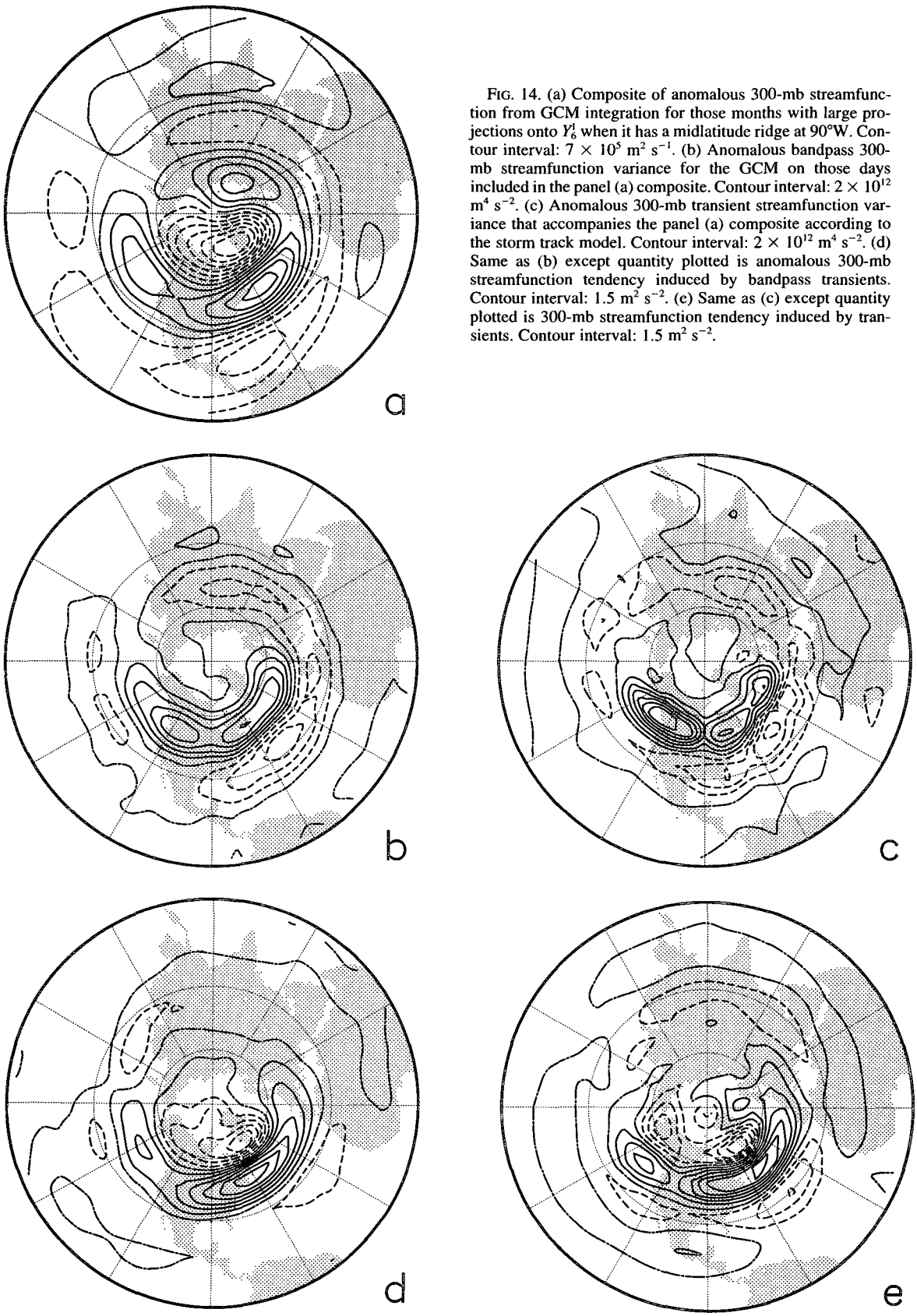

FIG. 14. (a) Composite of anomalous 300-mb streamfunction from GCM integration for those months with large projections onto Y_6^1 when it has a midlatitude ridge at 90°W. Contour interval: 7×10^5 m^2 s^{-1}. (b) Anomalous bandpass 300-mb streamfunction variance for the GCM on those days included in the panel (a) composite. Contour interval: 2×10^{12} m^4 s^{-2}. (c) Anomalous 300-mb transient streamfunction variance that accompanies the panel (a) composite according to the storm track model. Contour interval: 2×10^{12} m^4 s^{-2}. (d) Same as (b) except quantity plotted is anomalous 300-mb streamfunction tendency induced by bandpass transients. Contour interval: 1.5 m^2 s^{-2}. (e) Same as (c) except quantity plotted is 300-mb streamfunction tendency induced by transients. Contour interval: 1.5 m^2 s^{-2}.

dicates it to be a candidate for parameterization of heat fluxes as well.

Acknowledgments. This study has benefited from discussions the author has had with D. Baumhefner, B. Hoskins, R. Schnur, J. Tribbia, and H. von Storch. Comments on an earlier version of the manuscript by D. Baumhefner, A. Kasahara, Saravanan, J. Wallace, and two anonymous reviewers were also helpful. A. Mai produced the figures and L. Harper prepared the manuscript. This investigation was partially completed while the author was a visiting scientist at the Max Planck Institute for Meteorology. Partial support for this research has been provided at NCAR through the National Oceanic and Atmospheric Administration under Grant NA88AANRG0140.

REFERENCES

Blackmon, M. L., 1976: A climatological spectral study of the geopotential height of the Northern Hemisphere. *J. Atmos. Sci.*, **33,** 1607–1623.

Branstator, G., 1990: Low-frequency patterns induced by stationary waves. *J. Atmos. Sci.*, **47,** 629–648.

——, 1992: The maintenance of low-frequency atmospheric anomalies. *J. Atmos. Sci.*, **49,** 1924–1945.

Cai, M., and M. Mak, 1990: Symbiotic relation between planetary- and synoptic-scale waves. *J. Atmos. Sci.*, **47,** 2953–2968.

——, and H. M. van den Dool, 1991: Low-frequency waves and traveling storm tracks. Part I: Barotropic component. *J. Atmos. Sci.*, **48,** 1420–1436.

Dole, R. M., 1986: Persistent anomalies of the extratropical Northern Hemisphere wintertime circulation: Structure. *Mon. Wea. Rev.*, **114,** 178–207.

Egger, J., and H.-D. Schilling, 1983: On the theory of the long-term variability of the atmosphere. *J. Atmos. Sci.*, **40,** 1073–1085.

Farrell, F. B., 1989: Optimal excitation of baroclinic waves. *J. Atmos. Sci.*, **46,** 1193–1206.

Frederiksen, J. S., 1982: A unified three-dimensional instability theory of the onset of blocking and cyclogenesis. *J. Atmos. Sci.*, **39,** 969–982.

——, 1983: Disturbances and eddy fluxes in Northern Hemisphere flows: Instability of three-dimensional January and July flows. *J. Atmos. Sci.*, **40,** 836–855.

——, 1989: The role of instability during the onset of blocking and cyclogenesis in Northern Hemisphere synoptic flows. *J. Atmos. Sci.*, **46,** 1076–1092.

Hendon, H. H., and D. L. Hartmann, 1985: Variability in a nonlinear model of the atmosphere with zonally symmetric forcing. *J. Atmos. Sci.*, **42,** 2783–2797.

Hoskins, B. J., I. N. James, and G. H. White, 1983: The shape, propagation, and mean-flow interaction of large-scale weather systems. *J. Atmos. Sci.*, **40,** 1595–1612.

Illari, L., 1984: A diagnostic study of the potential vorticity in a warm blocking anticyclone. *J. Atmos. Sci.*, **41,** 3518–3526.

James, I. N., and L. J. Gray, 1986: Concerning the effect of surface drag on the circulation of a baroclinic planetary atmosphere. *Quart. J. Roy. Meteor. Soc.*, **112,** 1231–1250.

Karoly, D., 1983: Rossby wave propagation in a barotropic atmosphere. *Dyn. Atmos. Oceans,* **7,** 111–125.

Lau, N.-C., 1978: The observed structure of tropospheric stationary waves and the local balance of vorticity and heat. *J. Atmos. Sci.*, **36,** 996–1016.

——, 1981: A diagnostic study of recurrent meteorological anomalies appearing in a 15-year simulation with a GFDL general circulation model. *Mon. Wea. Rev.*, **109,** 2287–2311.

——, 1988: Variability of the observed midlatitude stormtracks in relation to low-frequency changes in the circulation pattern. *J. Atmos. Sci.*, **45,** 2718–2743.

——, and J. M. Wallace, 1983: On the distribution of horizontal transports by transient eddies in the Northern Hemisphere wintertime circulation. *J. Atmos. Sci.*, **36,** 1844–1861.

——, and E. O. Holopainen, 1984: Transient eddy forcing of the time-mean flow as identified by geopotential tendencies. *J. Atmos. Sci.*, **41,** 313–328.

——, and M. J. Nath, 1991: Variability of the baroclinic and barotropic transient eddy forcing associated with monthly changes in the midlatitude storm tracks. *J. Atmos. Sci.*, **48,** 2589–2613.

Lee, S., 1994: Localized storm tracks in the absence of local instability. *J. Atmos. Sci.*, in press.

Metz, W., 1989: Low-frequency anomalies of atmospheric flow and the effect of cyclone-scale eddies: A canonical correlation analysis. *J. Atmos. Sci.*, **46,** 1026–1041.

Mullen, S. L., 1987: Transient eddy forcing of blocking flows. *J. Atmos. Sci.*, **44,** 3–22.

Nakamura, N., 1993: Momentum flux, flow symmetry, and the nonlinear barotropic governor. *J. Atmos. Sci.*, **50,** 2159–2179.

Namias, J., 1953: Thirty-day forecasting: A review of a ten-year experiment. *Meteor. Monogr.*, No. 6, Amer. Meteor. Soc., 1–83.

Pettersen, S., 1956: *Weather Analysis and Forecasting.* McGraw-Hill, 428 pp.

Pitcher, E. J., R. C. Malone, V. Ramanathan, M. L. Blackmon, K. Puri, and W. Bourke, 1983: January and July simulations with a spectral general circulation model. *J. Atmos. Sci.*, **40,** 580–604.

Reinhold, B. B., and R. T. Pierrehumbert, 1982: Dynamics of weather regimes: Quasi-stationary waves and blocking. *Mon. Wea. Rev.*, **110,** 1105–1145.

Robertson, A. W., and W. Metz, 1989: Three-dimensional instability of persistent anomalous large-scale flows. *J. Atmos. Sci.*, **46,** 2783–2801.

——, and ——, 1990: Transient eddy feedbacks derived from linear theory and observations. *J. Atmos. Sci.*, **47,** 2743–2764.

Robinson, W., 1991: The dynamics of low-frequency variability in a simple model of the global atmosphere. *J. Atmos. Sci.*, **48,** 429–441.

Shutts, G. J., 1983: The propagation of eddies in diffluent jet streams: Eddy vorticity forcing of blocking flow fields. *Quart. J. Roy. Meteor. Soc.*, **109,** 737–761.

Simmons, A. J., and B. J. Hoskins, 1977: Baroclinic instability on the sphere: Solutions with a more realistic tropopause. *J. Atmos. Sci.*, **34,** 581–588.

——, and ——, 1978: The life cycles of some nonlinear baroclinic waves. *J. Atmos. Sci.*, **35,** 414–432.

Ting, M., and N.-C. Lau, 1993: A diagnostic and modeling study of the monthly mean wintertime anomalies appearing in a 100-year GCM experiment. *J. Atmos. Sci.*, **50,** 2845–2867.

Trenberth, K. E., and J. W. Hurrell, 1994: Decadal atmosphere–ocean variations in the Pacific. *Climate Dyn.*, **9,** 303–319.

Valdes, P. J., and B. J. Hoskins, 1988: Baroclinic instability of the zonally averaged flow with boundary-layer damping. *J. Atmos. Sci.*, **45,** 1584–1593.

Vautard, R., and B. Legras, 1988: On the source of midlatitude low-frequency variability. Part II: Nonlinear equilibration of weather regimes. *J. Atmos. Sci.*, **45,** 2845–2867.

Williamson, D. L., 1983: Description of NCAR Community Climate Model (CCM0B). NCAR Tech. Note, NCAR/TN-210+STR, 88 pp.